HHS Public Access

Author manuscript

Cell Stem Cell. Author manuscript; available in PMC 2024 August 03.

Published in final edited form as:

Cell Stem Cell. 2023 August 03; 30(8): 1054–1071.e8. doi:10.1016/j.stem.2023.07.010.

20-αHydroxycholesterol, an oxysterol in human breast milk, reverses mouse neonatal white matter injury through Gli-dependent oligodendrogenesis

Agnes S. Chao[1], **Pavle Matak**[1], **Kelly Pegram**[1], **James Powers**[1], **Collin Hutson**[1], **Rebecca Jo**[1], **Laura Dubois**[2], **J. Will Thompson**[2,3], **P. Brian Smith**[1], **Vaibhav Jain**[4,5], **Chunlei Liu**[6,7], **Noelle E. Younge**[1], **Blaire Rikard**[1], **Estefany Y. Reyes**[8], **Mari L. Shinohara**[8,9], **Simon G. Gregory**[4,5], **Ronald N. Goldberg**[1], **Eric J. Benner**[1,5,10,*]

[1]Division of Neonatology, Department of Pediatrics, Duke University Medical Center, the Jean and George Brumley, Jr. Neonatal-Perinatal Institute, Durham, NC 27710 USA.

[2]Duke Proteomics and Metabolomics Shared Resource, Center for Genomics and Computational Biology, School of Medicine, Duke University Medical Center, Durham, NC 27710 USA.

[3]Department of Pharmacology and Cancer Biology, School of Medicine, Duke University Medical Center, Durham, NC 27710 USA.

[4]Department of Neurology, Duke University Medical Center, Durham, NC 27710 USA.

[5]Duke Molecular Physiology Institute, Duke University Medical Center, Durham, NC 27710 USA.

[6]Department of Electrical Engineering and Computer Sciences, University of California, Berkeley, 94720 CA.

[7]Helen Wills Neuroscience Institute, University of California, Berkeley, 94720 CA.

[8]Department of Immunology, Duke University School of Medicine, Durham, NC 27710 USA.

[9]Department of Molecular Genetics and Microbiology, Duke University School of Medicine, Durham, NC 27710 USA.

[10]Lead Contact

Summary

White matter injuries (WMI) are the leading cause of neurologic impairment in infants born premature. There are no treatment options available. The most common forms of WMI in infants occur prior to the onset of normal myelination making its pathophysiology distinctive, thus requiring a tailored approach to treatment. Neonates present a unique opportunity to

*Correspondence: eric.benner@duke.edu (E.J.B).

Author Contributions. E.J.B. conceived/supervised project. A.S.C and P.M. designed and conducted experiments with help from K.P., J.P., C.H., and R.J. N.E.Y. and B.R. performed microbiology experiments. S.G.G. and V.J. performed scRNAseq. J.W.T. and L.D. performed mass spectrometry analysis. E.Y.R. and M.L.S. performed flow cytometry analyses. C.L. performed MRI and analysis. A.S.C., R.N.G, and E.J.B. interpreted the data and wrote the manuscript with input from all others.

Declaration of Interests. EJB and SGG are inventors on Duke University patent on oxysterol use in treating brain injury and inflammatory disease (US patent application number 15/325,039). The patent was licensed into Tellus Therapeutics and EJB and SGG are the scientific co-founders.

repair WMI due to a transient abundance of neural stem/progenitor cells (NSPCs) present in the germinal matrix with oligodendrogenic potential. We identified an endogenous oxysterol, 20-αHydroxycholesterol (20HC), in human maternal breast milk that induces oligodendrogenesis through a sonic hedgehog (shh), Gli-dependent mechanism. Following WMI in neonatal mice, injection of 20HC induced subventricular zone-derived oligodendrogenesis and improved myelination in the periventricular white matter resulting in improved motor outcomes. Targeting the oligodendrogenic potential of postnatal neural stem/progenitor cells in neonates with WMI may be further developed into a novel approach to mitigate this devastating complication of preterm birth.

Introduction

Preterm birth is a global health problem associated with high rates of morbidity and mortality[1]. While advances in neonatal care have improved survival among infants born at the earliest gestational ages, almost 80% of these infants survive with significant neurologic impairment[2]. Up to 10% of live births are impacted by premature birth. Survivors are at high risk for diffuse white matter injury (WMI), which is the most common neonatal brain injury leading to poor neurologic outcomes in these infants[3,4]. One important outcome linked to WMI is cerebral palsy (CP), the most common motor disability in childhood[5]. Moderate to severe motor disability has been reported in up to 10% of surviving premature infants[6–9]. In addition to motor disabilities, WMI can lead to broader deficits impacting cognitive, social-behavioral, and neurosensory outcomes. Despite the sheer magnitude of this problem, there are no treatment options available, only supportive care.

The period of highest risk for neonatal WMI occurs between 23–32 weeks post-conceptual age during a critical stage of white matter development that precedes myelination[10,11]. Cortical myelination begins around 34-weeks gestation and progresses in a caudal-to-rostral fashion[12,13]. This high-risk period is characterized by an abundance of pre-oligodendrocytes (pre-OLs) needed to provide the cellular source of myelinating oligodendrocytes[14]. Pre-OLs are more susceptible to inflammation and oxidative stress compared to their mature counterparts because they lack antioxidant enzymes (i.e., superoxide dismutase, glutathione peroxidase)[15,16]. While pre-OLs are susceptible to degeneration, immature cortical neurons, basal ganglia, and subcortical gray matter are more resistant to oxidative stress, resulting in lesions that preferentially involve the developing white matter. Necrotizing enterocolitis (NEC) or spontaneous intestinal perforations (SIP) are common complications in premature infants, and are linked to WMI. 50% of patients that survive NEC or SIP will develop significant neurodevelopmental impairment related to their WMI making this postnatal complication one of the most important encountered in this patient population[9,17,18].

While the neonatal period confers specific risks, it may also provide an opportunity for post-injury repair due to brain plasticity and abundance of neural stem/progenitor cells (NSPCs) within the germinal matrix that is not seen in older children or adults[19,20]. This structure contains NSPCs populations capable of giving rise to astrocytes and oligodendrocytes[21,22]. Premature infants are born when NSPCs residing in the germinal matrix are abundant and increasing gliogenesis[23]. The germinal matrix is a transient structure lining the ventricular

walls of the embryonic brain and is made up of the ventricular zone and the subventricular zone (SVZ). Early in development, the germinal matrix is responsible for proliferation of both neurons and glia. Neurogenesis occurs first, with new neurons proliferating in the germinal matrix and migrating radially to form the cortical plate and subsequent layers of the neocortex[24]. By 24-weeks gestation, down regulation of pro-neural factors and activation of pro-glial factors facilitate the production of astrocytes and oligodendrocytes[23]. This structure remains active through 32-weeks gestation, at which time it begins to involute radiographically and is not seen beyond 37-weeks. Developing therapies that replace lost pre-OLs may improve outcomes after neonatal WMI.

Therapeutic development in infants is complicated by appropriate concerns for safety. To address this challenge, we focused on identifying endogenous compounds with the potential to stimulate oligodendrogenesis. Oxysterols are endogenous oxidized cholesterols. Oxysterols have been detected in the blood, brain, and placenta of mammals but tissue specific functions are unknown[25,26]. Oxysterols are best known as endogenous ligands for Liver X Receptor (LXR)α and LXRβ and regulate cholesterol metabolism[27,28]. In addition to LXR signaling, multiple groups have recently identified select oxysterols as activators of the sonic hedgehog (shh) pathway[29–31]. Specifically, 20-αhydroxycholesterol (20HC) binds to the extracellular domain of smoothened leading to shh pathway activation and initiation of Gli Family Zinc Finger 1 (*Gli1*) transcription[29,30,32]. The shh pathway is a regulator of oligodendrocyte fate specification *in vivo* and enhances remyelination following injury in adult models of demyelination[33–36]. The impact of oxysterols on shh signaling forms the rationale for investigating their ability to modulate oligodendrogenesis following neonatal WMI. Because safety should be at the forefront of drug development in neonates, we characterized different oxysterols in human breast milk because it is rich in cholesterols. We identified 5 side-chain modified oxysterols in human milk, including 20HC, that served as candidates to further screen for shh activation and oligodendrocyte fate specification in NSPCs. The presence of these oxysterols in human milk suggests a high potential for safety in this extremely vulnerable population.

Results

Oxysterols in Human Maternal Breast Milk

Because breast milk is a rich source of cholesterol, we hypothesized that multiple oxysterols may be present. We used Ultraperformance Liquid Chromatography/Electrospray Ionization/Tandem Mass Spectrometry (UPLC/ESI/MS/MS) to identify oxysterols in breast milk[37]. Breast milk from healthy mothers within 2 months of a healthy full-term delivery. We detected millimolar levels of cholesterol (Figure S1A). We next examined breast milk for side-chain modified oxysterols including: 20HC, 22-hydroxycholesterol (22HC), 24-hydroxycholesterol (24HC), 25-hydroxycholesterol (25HC) and 27-hydroxycholesterol (27HC) (Figure S1B,C). Despite varying levels of detection for different oxysterols, we found nanomolar levels of each side chain-modified oxysterol in breast milk (Figure S1D-H). Our data demonstrate that breast fed neonates are routinely exposed to multiple oxysterols with no known adverse consequences.

20-αhydroxycholesterol (20HC) Induces Oligodendrogenesis *in vitro*

To identify candidate oxysterols among those found in breast milk for oligodendrogenic potential, we screened 20HC, 22HC, 24HC, 25HC, and 27HC at 1μM for shh activation in fibroblast-derived NIH 3T3 cells by measuring induction of *Gli1* mRNA. Hydroxylation at carbon 20 (20HC) had the strongest activity while hydroxylation at carbon 27 (27HC) failed to induce *Gli1* expression in NIH3T3 cells (Figure S1J). Our data allowed us to map side-chain hydroxylation sites with activity in the shh pathway onto a cholesterol backbone (Figure S1K). Transitioning to postnatal murine primary SVZ-derived NSPCs, we tested escalating doses of 20HC and 27HC for their differential ability to induce transcription of *Gli1* mRNA levels *in vitro*. In line with our NIH3T3 data, 20HC induced dose-dependent *Gli1* mRNA expression while 27HC did not increase *Gli1* mRNA expression (Figure S1L).

We next determined the impact of 20HC or 27HC on oligodendrocyte production in murine SVZ-derived NSPC populations *in vitro*. NSPCs were propagated in the presence of EGF and FGF as previously described[38] and treated with 1μM of oxysterol in chamber slides for 24 hours prior to EGF and FGF withdrawal. Oxysterol treatment continued for 3 additional days, after which cells were allowed to differentiate for a total of 15 days without further addition of oxysterol. Cells were fixed and immunostained for oligodendrocyte lineage markers, 2',3'-cyclic nucleoside 3'-phosphatase (CNPase) and myelin basic protein (MBP) (Figure 1A,B). Cell counting revealed that 20HC increased the number of $CNPase^+MBP^+$ cells within differentiated NSPC cultures. Conversely, 27HC did not alter the number of $CNPase^+MBP^+$ cells compared to controls (Figure 1B,C). Protein lysates from controls or those treated with either 1 μM 20HC or 27HC were probed for markers of oligodendrocyte lineages. 20HC significantly increased CNPase and MBP protein levels over control and 27HC treatment (Figure 1D-F). We next generated postnatal NSPC cultures from transgenic mice expressing membrane-anchored EGFP from the endogenous CNPase promoter in oligodendrocyte lineages[39]. Confocal analysis of differentiated NSPCs treated with 20HC confirmed that $EGFP^+$ cells co-localize with CNPase and MBP (Figure 1G). Flow cytometry experiments revealed that 20HC-treatement increased the percentage of $EGFP^+$ oligodendrocytes relative to vehicle control or 27HC-treated (Figure 1H).

To determine if 20HC acted on undifferentiated NSPCs or newly committed oligodendrocyte progenitor cell (OPC) populations, we cultured primary NSPCs as before but altered 20HC treatment timing. NSPCs were either treated with 20HC in media containing EGF and FGF 24 hours before withdrawal (Tx Time 1, Figure S2A), immediately upon withdrawal of EGF and FGF (Tx Time 2, Figure S2A), or 6 days after EGF and FGF withdrawal (Tx Time 3, Figure S2A). Cell numbers were analyzed following 15 days of differentiation using cell counting, and results show that the greatest increase in oligodendrocyte production is when 20HC treatment is initiated prior to EGF and FGF withdrawal suggesting 20HC targets uncommitted NSPCs (Figure S2B). To further exclude the possibility that 20HC induces proliferation in oligodendrocyte progenitor cells (OPCs) *in vitro*, we isolated primary $A2B5^+$ OPCs from postnatal day 5–7 (p5–7) mice using anti-A2B5 magnetic beads (Figure S2C). OPCs were propagated in proliferation media containing PDGF and treated with escalating doses of 20HC (0.1–1μM). Cell proliferation was analyzed using CellTrace Violet. Cells were cultured for 3 days after CellTrace Violet exposure then analyzed by flow

cytometry. There was no significant difference in proliferation of control OPCs compared to 20HC treated cells at any dose tested (Figure S2D,E). Additionally, 20HC did not change the proliferation when the experiment was conducted on OPCs in differentiation media that lacks PDGF (Figure S2D,F). In fact, there was a trend toward decreased proliferation after 20HC treatment. Together, these results further suggest that 20HC does not induce proliferation in OPCs and supports our conclusion that the increased oligodendrocyte production resulted from NSPCs changing their fate and not an expansion of committed oligodendrocyte progenitors.

We also investigated the impact of 20HC on additional cell lineages generated during *in vitro* differentiation of SVZ-derived NSPCs. We cultured NSPCs and treated them with escalating doses of 20HC and allowed them to differentiate for 5 days. On day 5, cells were fixed and immunostained for oligodendrocyte transcription factor 2 (Olig2), glial fibrillary acidic protein (GFAP), and doublecortin (Dcx) (Figure S2G). In separate experiments, qPCR analysis for the same oligodendrocyte, astrocyte, and neuronal markers was performed. There was a dose dependent increase in Olig2 mRNA in response to 20HC (Figure S2H). However, our analysis showed no significant difference in the neuronal marker, Dcx, between control and 20HC treated groups (Figure S2I). We did observe a 20HC dose dependent decrease in astrocyte marker, GFAP (Figure S2J). These results suggest that 20HC-induced oligodendrogenesis does not affect NSPC-derived neurogenesis but may drive cell fate away from astrocyte lineages.

We then applied a single cell droplet sequencing approach (10xgenomics, Pleasanton, CA) to compare early emerging oligodendrocyte progenitor populations within 20HC-treated and vehicle-treated NSPCs immediately following 20HC dosing. NSPCs were expanded into vehicle control (DMSO) or 1μM 20HC-treated groups. 3 days after EGF and FGF withdrawal we sequenced genes over 15,000 cells combined and used Uniform Manifold Approximation and Projection (UMAP) dimensionality reduction to condense the data into a 2D space and segregate cell groups based on gene expression profiles (Figure 2A). We identified cell clusters (Figure 2B), including an emerging oligodendrocyte committed population based on expression of Platelet Derived Growth Factor Receptor α (*Pdgfra*), Chondroitin Sulfate Proteoglycan 4 (*Cspg4)*, Oligodendrocyte Transcription Factor 1 (*Olig1*), Olig2, and Sox10 (Figure S3A-E). Olig1, Olig2, Pdgfrα, Sox10 and Cspg4 (NG2) are known markers of the oligodendrocyte lineage. Analysis of UMAP plots comparing the size of the oligodendrocyte committed lineages relative to the entire population revealed a 30% increase in oligodendrocyte committed progenitors in the 20HC-treated cells compared to controls at this early time point (Figure 2C). As a secondary measure, we treated NSPC cultures with vehicle or escalating doses of 20HC and analyzed mRNA levels of *PDGFRα, Cspg4, Olig1,* and *Olig2* by qPCR on day 3 of treatment. All 4 genes followed a 20HC dose dependent increase when compared to controls, supporting our single cell analysis above (Figure 2D). We also immunostained differentiating NSPC cultures for Olig2 and PDGFRα at 5 days of differentiation to assess the production of OPCs (Figure S3F,G). To better understand what signaling crosstalk via membrane-bound receptors and their soluble ligands are occurring in our NSPC cultures following 20HC treatment *in vitro*, we performed a CellChat analysis[40]. CellChat identified interactions between cell type in both control and 20HC-treated groups (Figure 2E-H). Observations include the production of

PDGF from FoxJ1$^+$ ependymal cells in culture and the reciprocal activation of the PDGFRα pathway on OPCs following 20HC treatment. Furthermore, 20HC treatment increased NSPC signaling within the thrombospondin (THBS) pathway which has been implicated in Notch signaling[38,41].

Pseudobulk RNAseq analysis in 20HC-treated cells compared to control revealed increased expression of multiple genes, including Wdr89, Nme2 and Grcc10, and decreased expression of multiple genes, including Fbxo2 and Hmgn1 (Figure S3H). Of interest, Fbxo2 expression is associated with astrocytes and is upregulated in astrocytes during disease[42]. Hmgn1 regulates NSPC fate specification of the astrocytic lineage[43]. Analysis of 20HC-treated NSPCs compared to control showed increased expression of Wdr89 and Grcc10, and decreased expression of Hmgn1 (Figure S3I). Analysis of 20HC-treated OPCs compared to control revealed increased expression of Wdr89 and Nme2, and decreased expression of Gfap and Hmgn1 (Figure S3J). 20HC mediated Wdr89 expression was increased in all 3 analyses although little is known about its function. Decreased expression of Fbxo2 and Hmgn1 in 20HC-treated cells compared to control suggests a downregulation of astrocyte production in response to 20HC. These transcriptomic results support the conclusion that treatment with 20HC induces oligodendrocyte fate specification, perhaps at the expense of the astrocytic lineage.

Molecular Mechanisms of 20HC-Mediated Oligodendrogenesis

Because oxysterols are classically known as LXR agonists, we assessed its role in 20HC-induced oligodendrogenesis. At 1μM, we found that 20HC treatment induced the transcription of both the ATP-binding cassette sub-family A member 1 (*Abca1*) and ATP-binding cassette sub-family G member 1 (*Abcg1*) genes consistent with LXR activation. As an oxysterol control, we included 22HC as a known LXR antagonist[44,45] and did not observe an induction of *Abca1* or *Abcg1* as expected in primary NSPCs (Figure S4A,B). To antagonize 20HC-mediated LXR activation *in vitro*, we utilized an LXRα and LXRβ antagonist, GSK2033[46]. Treatment of NSPCs with 100nM GSK2033 attenuated 20HC-induced *Abca1* and *Abcg1* mRNA induction (Figure S4A,B). We next tested if LXR inhibition would impact 20HC-induced oligodendrogenesis *in vitro* by immunostaining CNPase$^+$MBP$^+$ oligodendrocytes in 15-day differentiated cultures (Figure S4C). We observed 20HC-induced oligodendrogenesis as before. Inhibition of LXR with GSK2033 did not disrupt the generation of oligodendrocytes *in vitro* (Figure S4D). Additionally, inhibition of LXR signaling with GSK2033 failed to disrupt oxysterol-mediated increases in CNPase or MBP protein levels *in vitro* (Figure S4E-G). These results are not supportive of an LXR role in 20HC-mediated oligodendrocyte fate specification.

We next interrogated the role of shh signaling in oxysterol-induced oligodendrogenesis. Shh signaling is the most well studied molecular pathway influencing NSPC fate switch into the oligodendrocyte lineage[47,48]. We treated NSPCs with 300ng/ml shh in vitro and observed increased numbers of CNPase$^+$ oligodendrocytes and olig2 and MBP protein levels (Figure S4H-K). Because Gli1 and Gli2 are downstream transcription factors of the shh pathway, we used the Gli1 and Gli2 inhibitor, GANT61[49] to block shh-induced oligodendrogenesis (Figure S4I-K). We then examined the ability of GANT61 to block

20HC-induced oligodendrogenesis *in vitro*. NSPCs were and exposed to media control, 5μM GANT61, 1μM 20HC or 20HC+GANT61, and allowed to differentiate as before. Following 15 days of differentiation, fixed cells were stained for CNPase and counterstained with DAPI (Figure 3A). Cell counting revealed an increased number of $CNPase^{+}$ cells in 20HC-treated cultures. GANT61 blocked 20HC-mediated increases in oligodendrocyte numbers (Figure 3B). Protein lysates then were probed for CNPase and MBP confirming that GANT61 treatment abolished 20HC-mediated oligodendrogenesis *in vitro* (Figure 3C-E). Together, these data suggested a functional role for Gli1 and/or Gli2 in 20HC-dependent oligodendrogenesis.

We next used a transgenic approach to generate newborn pups deficient in either *Gli1* or *Gli2* using Gli1-LacZ or Gli2-LacZ knock in alleles[50]. Heterozygous $Gli1\text{-}LacZ^{KI}$ males were crossed to heterozygous $Gli1\text{-}LacZ^{KI}$ females to produce $Gli1^{+/+}(Gli1^{WT})$, $Gli1^{+/KI}(Gli1^{Het})$, and $Gli1^{KI/KI}$ $(Gli1^{KO})$ NSPC cultures. NSPCs from these Gli1 genotypes were propagated in EGF and FGF and then exposed to vehicle or 1μM 20HC as before. After 15 days of differentiation, we found increased levels of CNPase and MBP protein in differentiated NSPC cultures from $Gli1^{WT}$ and $Gli1^{Het}$ pups following 20HC-treatment. However, differentiated NSPCs generated from $Gli1^{KO}$ pups showed a significant reduction in CNPase and MBP levels despite 20HC treatment (Figure 3F-H). A similar approach using $Gli2\text{-}LacZ^{KI}$ alleles was used to generate these same Gli2 genotypes and perform western blots to measure CNPase and MBP. These Gli2 genotypes revealed a similar pattern compared to our Gli1 studies although the effect of $Gli2^{KO}$ on 20HC-induced oligodendrogenesis was more profound compared to $Gli1^{KO}$ (Figure 3I-K). This suggests that Gli2 transcription is essential for 20HC-induced oligodendrogenesis and may be able to compensate for Gli1 function when knocked out. Because Gli2 deletion resulted in the most robust change in CNPase and MBP levels, we repeated the experiments for cell analysis, immunostaining for CNPase. Differentiation of primary $Gli2^{WT}$, $Gli2^{Het}$, or $Gli2^{KO}$ NSPCs in untreated control media generated similar cell morphology and numbers of $CNPase^{+}$ oligodendrocytes demonstrating that $Gli2^{KO}$ did not disrupt baseline oligodendrocyte production (Figure 3L,M). However, when stimulated with 20HC, NSPCs deficient in Gli2 did not increase their oligodendrocyte fate specification (Figure 3L,N). Despite similar oligodendrocyte numbers and morphology of $Gli2^{KO}$ cells observed *in vitro*, we performed additional testing to determine if Gli2 deficient oligodendrocytes behave normally when compared to their WT counterparts. Thyroid hormone (3,3',5-Triiodo-L-thyronine, T3) is a well-known inducer of oligodendrocyte maturation. We cultured NSPCs from $Gli2^{WT}$ and $Gli2^{KO}$ pups as above and treated with vehicle or 50nM T3. After 12 days of differentiation, cells were fixed and stained with CNPase and MBP. Using Sholl analysis to characterize the morphology of cells and quantify their complexity showed that oligodendrocytes from both $Gli2^{WT}$ and $Gli2^{KO}$ mice treated with T3 were similarly more complex and mature compared to control (Figure 3O,P). Compared to $Gli2^{WT}$ NSPCs, NSPCs from $Gli2^{KO}$ mice give rise to similar numbers of OPCs that mature as expected in response to T3 *in vitro*. Together, these results demonstrate that deleting Gli2 impairs 20HC-induced oligodendrocyte fate specification but does not affect the ability of other endogenous molecules, such as T3, to promote their differentiation into mature oligodendrocytes.

Neonatal intestinal perforation inflammatory brain injury model

To next explored the efficacy of 20HC in a clinically relevant animal model of neonatal intestinal perforation and sepsis[51,52]. Briefly, cecal contents (stool) from young (p20-p22) stool donors were injected into the peritoneal cavity of recipient mice on p5 to induce peritonitis (Figure S5A). Microbiota analysis in donor stool samples (n=9) was performed to understand the diversity of organisms injected into the peritoneal cavity (Figure S5B). We injected escalating cecal slurry doses (500–1000mg/kg) into the recipient mice on p5 and determined survival (Figure S5C). Because a stool dose of 800mg/kg only resulted in ~5% death rate, we conducted the remaining studies at this dose. To determine if peritoneal injection of stool resulted in bacterial seeding of systemic organs, we euthanized pups 72 hours after stool injection and their spleen, lung and SVZ were dissected and homogenized for bacterial culture. Plating these homogenates on MacConkey agar to select for gram negative bacteria, we found that 8/8 injected mice grew colonies from the spleen, 7/8 mice grew colonies from the lung, and 4/8 mice had positive cultures from the SVZ (Figure S5D). 16S rRNA sequencing of the colonies obtained from the SVZ identified them as *Escherichia* genus matching sequences obtained from the stool samples. Control mice (n=6) showed no growth in any organs tested. We then examined the inflammatory cytokine profile by qPCR in the systemic circulation (spleen) and the central nervous system (CNS) at 2 days post peritoneal stool injection (p7). Stool-induced peritonitis resulted in increased expression of *Tnfα, IL-6, IL-1β,* and numerous chemokines in the systemic circulation and elevations of *IL-1β* and *IL-17α* in the CNS (Figure S5E).

To determine the global impact of modeled intestinal perforation on neonatal brain injury, we performed brain MRI. Sepsis was induced in mice on p5. 4 days later (p9) control mice (n=2) and septic littermates (n=2) were perfusion fixed with contrast and imaged (Figure S5F). We observed diffusion changes within the periventricular white matter regions (Figure S5G-I). Quantification of diffusivity changes from 20 sites/mouse within each region of interest revealed a more pronounced change in white matter structures compared to cortical gray matter regions (Figure S5J-M). Septic mice showed a marked increase of diffusivity in the corpus callosum (CC), suggesting a loss of cellularity (e.g. loss of oligodendrocytes) and a possible reduction of myelination. To further assess myelination, we employed quantitative susceptibility mapping MR sequences. Diamagnetic susceptibility of white matter is caused by myelin lipids and has successfully been used to assess myelin architecture including in neonates[53–55]. Higher myelination results in more diamagnetic susceptibility in white matter. In our control mice, we observed more diamagnetic properties in the CC compared to our septic mice at this time point (Figure S6A). Averaged changes in magnetic susceptibility revealed predominant changes in the periventricular CC relative to cortical regions (Figure S6B,C). The finding of increased diffusion and the change in magnetic susceptibility strongly suggested myelin deficits with possible axonal injury in this structure.

We then performed experiments to quantify the numbers of mature oligodendrocytes by stereology on p25. Coronal tissue sections spanning the entire ventricular region were immunostained for CC1 and Olig2 and every fourth section was counted (Figure S6D). We identified a stool dose-dependent decrease in the number of $CC1^{+}Olig2^{+}$ oligodendrocytes within the CC that aligns with the changes we observed on MRI (Figure S6E,F). In

summary, injection of stool into the peritoneal cavity to model a neonatal intestinal perforation resulted in stool-derived bacteria seeding multiple organ systems accompanied with systemic and neuroinflammation. Surviving mice developed both diffusion changes and changes in magnetic susceptibility located preferentially in the periventricular white matter structures, which correlated with oligodendrocyte deficits at p25.

20HC Rescues Neonatal Inflammatory White Matter Injury *in vivo*

We next developed a protocol to analyze cell death, OPC numbers, and mature oligodendrocyte numbers at various time points following p5 induction of WMI in treated and untreated mice (Figure 4A). *IL-1β* gene expression at p7 (24 hours after treatment) and did not observe a significant impact on this proinflammatory cytokine (Figure 4B). We next determined the numbers of PDGFRα+ OPCs in uninjured controls, vehicle-treated septic mice, and septic mice treated with 5 days of 20HC (100mg/kg/day). This analysis was conducted 24 hours following the final dose of 20HC on p11. Using stereology, we observed a reduction in OPC numbers in septic animals compared to controls. However, we did observe an increase in the number of OPCs in septic animals treated with 20HC (Figure S7A,B). Combining PDGFRα immunostaining with proliferation marker Ki67, we determined that the fraction of OPCs undergoing proliferation at this time point was increased in 20HC-treated animals (Figure S7C,D). To address whether 20HC impacts the number of dying OPCs, we induced sepsis on p5 and initiated daily treatment (vehicle or 20HC) earlier at 8 hours post-stool injection. Two days later (p7), we immunostained brains for PDGFRα and activated caspase-3 and counted the number of double-positive cells in the periventricular CC and subcortical white matter. We observed rare caspase-3^+ OPCs in the control animals and increased numbers in septic animals (Figure 4C,D). However, there was no difference in caspase-3^+ cells in septic animals treated with 20HC compared to septic animals treated with vehicle control at this time point suggesting that 20HC therapy does not alter cell death after injury (Figure 4C,D).

To determine if 20HC treatment impacted the number of mature oligodendrocytes, we compared control mice, vehicle-treated septic mice, and septic mice randomized to 20HC treatment at 100mg/kg/day for 5 days. To determine if treatment alters cholesterol or 20HC levels in the CNS, we measured serum and brain levels of these compounds at 24 hours after mice completed a 5-day 20HC treatment. Using mass spectrometry, we observed no significant difference in brain cholesterol levels following treatment (Figure S7E). However, we did observe increased 20HC levels in the serum and brains of uninjured and septic mice treated with 20HC compared to vehicle-treated control and septic mice (Figure S7F,G).We included 27HC treatment at the same dose as an additional control. Treatment dosing began 24 hours after stool injection. We processed brains for oligodendrocyte stereology as before at p25 (Figure 4E). As expected, the number of mature $CC1^+Olig2^+$ oligodendrocytes in the sepsis group decreased compared to uninjured control mice (Figure 4F). However, treatment with 20HC resulted in increased numbers of periventricular $CC1^+Olig2^+$ oligodendrocytes when compared to either vehicle alone or the non-oligodendrogenic 27HC (Figure 4F). Subsequent experiments using 20HC were analyzed at the later time point of p60 to determine if this benefit was permanent. The analysis at this later time point was similar to numbers obtained at p25 with 20HC showing a significant increase in numbers of

mature oligodendrocytes compared to vehicle-treated septic mice (Figure 4G). Subsequent experiments using decreasing doses of 20HC from 50 to 1 mg/kg/day revealed a dose-dependent response to 20HC and further identified 50mg/kg/day for 5 days as the minimum dose required for complete rescue of oligodendrocyte cell numbers back to control levels (Figure 4H).

To investigate the impact of sepsis and 20HC (100mg/kg/day) treatment on myelination, we stained sagittal sections with Black Gold to identify subcortical myelinated fibers at p25 (Figure 5A,B). To quantify subcortical myelinated fiber length, we utilized an unbiased Space Balls stereological probe. Space Balls uses systematic random sampling to determine the end-to-end length of linear objects in tissue, in this case myelinated fibers. Our analysis revealed a significant decrease in overall myelinated fiber length in the subcortical white matter in septic animals treated with vehicle alone when compared to uninjured controls. However, septic littermates treated with 20HC demonstrated increased myelinated fiber length throughout comparable subcortical regions (Figure 5C). We next performed transmission electron microscopy (TEM) on midline sagittal sections in the CC in uninjured controls, septic mice, and septic mice treated with 20HC at p20 (Figure 5D). We observed an increase in g-ratio in our septic cohort that normalized to control levels with 20HC treatment (Figure 5E). Moreover, we observed decreased numbers of myelinated axons in the septic animals compared to control littermates. Following 20HC treatment, we observed an increased number of myelinated axons relative to vehicle-treated animals (Figure 5F). Together, these data demonstrate increased numbers of mature oligodendrocytes that persist into adulthood and improved myelination in the periventricular and subcortical white matter in septic mice following treatment with 20HC.

To assess motor outcomes, we utilized our CatWalk gait analysis system. We generated control littermates and mice that were injected with cecal slurry at p5 as above. These mice were randomized into vehicle control or 20HC-treated groups (100mg/kg/day x 5 days) and performed gait analysis at 2 months (p60) of age. Mice that were treated with vehicle alone demonstrated a significant reduction in their regularity index. Deficits in regularity index were corrected in mice treated with 20HC (Figure 6A,B and Supplemental Video 1, $p<0.0001$). Regularity index is a measure of interlimb coordination and motor planning. We also detected an abnormal swing time and step cycles in the forelimbs compared to hind limbs in septic mice compared to controls. All forelimb gait deficits were corrected in 20HC-treated animals (Figure 6D-K). This gait analysis showed that neonatal septic mice treated with 20HC had improved motor function that persisted into adulthood.

20HC Enhanced SVZ-Derived Oligodendrogenesis *in vivo*

Connecting these *in vivo* results to our *in vitro* observations on mechanism in NSPCs, we utilized the Nestin-CreER^{T2} allele to lineage trace SVZ NSPCs following injury[56]. This genetic strategy allows us to determine if 20HC treatment *in vivo* results in SVZ-derived oligodendrogenesis that contribute to recovery in the affected periventricular white matter regions. We crossed the Nestin-CreER^{T2} allele to the R26r-TdTomato reporter line to lineage trace these postnatal NSPCs *in vivo*. Tamoxifen injection on p4 and immunohistochemical analysis 3 days later revealed TdTomato recombination in

Sox2$^+$Nestin$^+$ SVZ NSPCs (Figure 7A,B). As a control, analysis of transgenic mice that did not receive tamoxifen injection but received 5 days of 20HC treatment did not show any detectable levels of R26r-TdTomato recombination (Figure S8A,B). 3 days after tamoxifen injection, TdTomato$^+$ cells present in the periventricular white matter co-localized with GFAP$^+$ astrocytes but not NG2$^+$ OPCs, demonstrating that p4 tamoxifen injection does not label cells in the OPC lineage (Figure S8C-E).

To lineage trace SVZ-derived NSPCs *in vivo*, Nestin-CreER^{T2};R26r-TdTomato pups were injected with tamoxifen on p4. Mice were randomized into four groups: uninjured control mice, uninjured mice with 20HC treatment, septic mice treated with vehicle alone, or septic mice treated with 20HC (100mg/kg/day x 5 days, Figure 7C). At p25, brains were perfusion fixed and coronal sections spanning the lateral ventricles were immunostained for TdTomato and CC1 (Figure 7D). Stereology was used to enumerate total numbers of CC1$^+$ oligodendrocytes and confirmed a loss of periventricular oligodendrocytes in septic animals that was improved after 20HC treatment (Figure 7E). When looking at new SVZ-derived cell output (Td-Tomato$^+$), we noted that there are increased numbers of SVZ-derived cells in all treatment groups compared to control. However, only in the 20HC-treated groups did we see increased numbers of TdTomato$^+$CC1$^+$ oligodendrocytes (Figure 7F). 20HC treatment of uninjured mice did not significantly change the total number of mature oligodendrocytes at p25 but did increase the fraction of SVZ-derived (TdTomato$^+$) cells represented in this population (Figure 7E,F). As expected, the vehicle-treated septic mice had a reduction in total CC1$^+$ oligodendrocyte numbers and the number of CC1$^+$ oligodendrocytes that co-localized with TdTomato was similar to numbers seen in control mice (Figure 7E,F). This suggests that the SVZ did not significantly contribute new oligodendrocytes after injury in the absence of treatment. In contrast, septic mice treated with 20HC had normalized total CC1$^+$ oligodendrocyte numbers and had significantly more CC1$^+$Tomato$^+$ (newly generated) oligodendrocytes when compared to control, vehicle-treated septic mice ($p<0.0001$) or uninjured 20HC-treated mice ($p<0.05$) (Figure 7E,F). These data demonstrate that 20HC-mediated recovery of oligodendrocyte deficit is mediated, at least in part, through 20HC-induced SVZ-derived oligodendrogenesis *in vivo*.

Discussion

Diffuse WMI is the most common neonatal brain injury leading to poor neurologic outcomes in premature infants. Systemic inflammation from infection is a risk factor linked to these outcomes, and there are no treatment options available. Developing new therapeutics for neonates is challenging due to appropriate concerns for safety. We identified a potential therapeutic use for an endogenous oxysterol, 20HC, in neonatal WMI. 20HC promotes oligodendrocyte fate specification in postnatal SVZ-derived NSPCs *in vitro*. Using pharmacologic and genetic approaches, we identified shh signaling through Gli2 as the key molecular mechanism driving the production of new oligodendrocytes from NSPCs *in vitro*. Using a clinically relevant model of inflammatory neonatal WMI, we found that treatment with 20HC increases numbers of mature oligodendrocytes, improves myelination, and rescues motor deficits. Modeled intestinal perforation induces an inflammatory WMI resulting in a loss of periventricular OPCs, hypomyelination, and motor deficits that persist through adulthood (p60). 20HC treatment resulted in increased number of mature

oligodendrocytes, improved myelination, and motor outcomes at 2 months. Using the Nestin CreER^{T2} allele to lineage trace postnatal NSPCs, we confirmed that NSPC production of new oligodendrocytes following 20HC treatment is one mechanism through which 20HC rescues neonatal WMI *in vivo*. We found no significant differences in cell death (caspase-3$^+$ cells) between vehicle-treated and 20HC-treated injured mice, suggesting that the therapeutic effect of 20HC is not due to increased survival of OPCs. The approach presented here appears to replace cells after injury by targeting NSPC pools present in preterm neonates. This is an important distinction because the precise timing of brain injury in preterm infants is often difficult or impossible to determine and therapeutic windows for "protective" approaches are often short due to the need to intervene prior to cell death.

There is significant controversy in the field surrounding the underlying mechanism that results in preterm brain injury, including diffuse WMI. Studies in human tissue suggest that myelination failure is a result of arrested oligodendrocyte lineage progression after injury[57,58], while others suggest that hypomyelination is due to oligodendrocyte progenitor cell death[59]. 48 hours after modeled intestinal perforation in our model of inflammatory WMI, we found significantly increased numbers of caspase-3$^+$PDGFRα+ cells in the periventricular white matter of septic mice compared to control, which is indicative of apoptotic cell death after injury in early OPCs. These results are similar to the findings of hypoxic-ischemic cellular degeneration of late OPCs by Back et al. in early periventricular WMI[16]. In contrast, studies in which cell death was not observed were performed in post-mortem tissue of infants with chronic WMI[57,58]. Cell death may not have been observed due to tissue analysis after the acute phase of injury or alternative mechanisms (non-apoptotic) of cell death[60]. Unchanged or increased numbers of immature oligodendrocytes observed in these studies may be secondary to increased progenitor cell proliferation or failure of maturation of surviving cells. Nevertheless, the underlying pathophysiology of neonatal WMI is likely multifactorial, due to a combination of oligodendrocyte progenitor cell death, regeneration, and maturation arrest, warranting further investigation.

Shh signaling known to play a significant role in oligodendrocyte fate specification. When shh is activated, it results in downstream target gene transcription via Gli1 and Gli2. Previous work has demonstrated that shh signaling is necessary for Olig gene expression during early stages of oligodendrocyte development *in vivo*[33–36]. Of note, an interesting study using a Gli1/Gli2 inhibitor, GANT61, demonstrated enhanced oligodendrocyte production in a narrow subset of Gli1$^+$ SVZ NSPCs in adult toxin models of myelin injury[61]. In contrast, our study demonstrates that 20HC treatment increases oligodendrocyte fate specification by exploiting the shh activation properties of oxysterols and subsequent downstream activation of Gli1 and particularly Gli2. Our *in vitro* experiments showed that GANT61 disrupted 20HC-dependent oligodendrocyte fate specification. Subsequent genetic approaches to delete Gli1 or Gli2 confirmed their critical roles in 20HC-induced oligodendrocyte fate specification, with Gli2 deletion having the most profound impact. At no time in our investigation did we observe an increase in neonatal NSPC-derived oligodendrogenesis following a disruption of shh signaling with GANT61, but we did observe a small but significant increase in CNPase$^+$ oligodendrocyte committed cells following deletion of Gli2. Our studies differ most notably in the focus on Gli2 versus Gli1 and importantly, the age of mice studied. Here we used neonatal mice whose shh-responsive

(Gli1$^+$) SVZ NSPC population differs greatly from that observed in the adult animal[62], which likely accounts for the difference in our results.

Therapeutic development for neonates must have safety in the forefront, thus discovering therapeutic uses of natural compounds found in breast milk is an appealing strategy. 20HC has been described in human placenta and the mammalian CNS and here we report its presence in human breast milk. There is a significant body of literature discussing the benefit of breast milk feeding over formula on neurodevelopmental outcomes in preterm infants, when controlling for environmental and social factors[63]. Breast feeding is associated with improved connectivity observed on MRI in survivors of preterm birth[64]. Moreover, breastfeeding duration is associated with improved Bayley scores at 12, 18 and 30 months corrected age, alongside improved structural connectivity, and myelin architecture in several brain regions[65–67]. However, the mechanism underlying improved neurodevelopmental outcomes remains unknown. Some have suggested specific nutritional components of breast milk, such as long chain polyunsaturated fatty acids, are the key factor, while others attribute improved neurodevelopmental outcomes to the decreased risk of NEC in preterm infants[66]. Importantly, data presented here does not directly address a role for oxysterols in human breast milk as a mechanism for the observed improvement of neurodevelopmental outcomes in breastfed infants. Notably, our oxysterol approach used higher exposures and a different route of administration when compared to breastfed infants. Exploration of the role of endogenous oxysterols in breast milk on neurodevelopmental outcomes will require future investigation. Our purpose for including the oxysterol levels in breast milk in the present study is demonstrate infants exposures to this class of molecules and that there is a safe exposure level in the preterm infant.

Limitations of the Study

As with all pre-clinical studies, our results are limited by our animal model. Our model of inflammatory neonatal WMI is induced in otherwise healthy mice. Preterm infants that develop intestinal perforation and subsequent diffuse WMI often also have co-morbidities that may include intraventricular hemorrhage and developing chronic lung disease, which may also affect neurodevelopmental outcomes. Thus, there may be additional confounding or complicating factors that we are unable to account for in this study.

Supplementary Material

Refer to Web version on PubMed Central for supplementary material.

Acknowledgements.

We thank Mari Porter, Marki Allison, Dr. Kimberly Fisher, and Joanne Finkle for help obtaining breast milk samples. Work was supported by Jean and George Brumley Jr. Neonatal Perinatal Research Institute, the Zeist Foundation, Children’s Miracle Network Hospitals partnerships and programs benefiting Duke Children’s, and grants from the National Institutes of Health (1R01NS114578) to EJB, T32HD094671 to ASC, K12HD043494 (PI Reed) and T32HD043728 (PI Goldberg). Additional support from the Duke Scholars Award from the School of Medicine, National Institutes of Health (NIH) through grants R01AG070826 and R01MH127104, Duke University Center for In Vivo Microscopy, NIH P41EB015897(C.L). E.J.B. was supported by the National Center for Advancing Translational Sciences (NCATS), National Institutes of Health, through Grant Award Number 1UL1-TR002553 (content is solely the responsibility of the authors and does not necessarily represent the official views of the NIH).

References:

1. Liu L, Oza S, Hogan D, Chu Y, Perin J, Zhu J, Lawn JE, Cousens S, Mathers C, and Black RE (2016). Global, regional, and national causes of under-5 mortality in 2000–15: an updated systematic analysis with implications for the Sustainable Development Goals. The Lancet 388, 3027–3035. 10.1016/s0140-6736(16)31593-8.
2. Younge N, Goldstein RF, Bann CM, Hintz SR, Patel RM, Smith PB, Bell EF, Rysavy MA, Duncan AF, Vohr BR, et al. (2017). Survival and Neurodevelopmental Outcomes among Periviable Infants. N Engl J Med 376, 617–628. 10.1056/NEJMoa1605566. [PubMed: 28199816]
3. Volpe JJ (2009). Brain injury in premature infants: a complex amalgam of destructive and developmental disturbances. The Lancet Neurology 8, 110–124. 10.1016/s1474-4422(08)70294-1. [PubMed: 19081519]
4. Woodward LJ, Clark CA, Bora S, and Inder TE (2012). Neonatal white matter abnormalities an important predictor of neurocognitive outcome for very preterm children. PLoS One 7, e51879. 10.1371/journal.pone.0051879. [PubMed: 23284800]
5. Colver A, Fairhurst C, and Pharoah POD (2014). Cerebral palsy. The Lancet 383, 1240–1249. 10.1016/s0140-6736(13)61835-8.
6. Beaino G, Khoshnood B, Kaminski M, Pierrat V, Marret S, Matis J, Ledesert B, Thiriez G, Fresson J, Roze JC, et al. (2010). Predictors of cerebral palsy in very preterm infants: the EPIPAGE prospective population-based cohort study. Dev Med Child Neurol 52, e119–125. 10.1111/j.1469-8749.2010.03612.x. [PubMed: 20163431]
7. Hack M, Taylor HG, Drotar D, Schluchter M, Cartar L, Andreias L, Wilson-Costello D, and Klein N (2005). Chronic conditions, functional limitations, and special health care needs of school-aged children born with extremely low-birth-weight in the 1990s. JAMA 294, 318–325. 10.1001/jama.294.3.318. [PubMed: 16030276]
8. Mercier CE, Dunn MS, Ferrelli KR, Howard DB, Soll RF, and Vermont Oxford Network EIF-USG (2010). Neurodevelopmental outcome of extremely low birth weight infants from the Vermont Oxford network: 1998–2003. Neonatology 97, 329–338. 10.1159/000260136. [PubMed: 19940516]
9. Wadhawan R, Oh W, Hintz SR, Blakely ML, Das A, Bell EF, Saha S, Laptook AR, Shankaran S, Stoll BJ, et al. (2014). Neurodevelopmental outcomes of extremely low birth weight infants with spontaneous intestinal perforation or surgical necrotizing enterocolitis. J Perinatol 34, 64–70. 10.1038/jp.2013.128. [PubMed: 24135709]
10. Back SA, Luo NL, Borenstein NS, Volpe JJ, and Kinney HC (2002). Arrested oligodendrocyte lineage progression during human cerebral white matter development: dissociation between the timing of progenitor differentiation and myelinogenesis. J Neuropathol Exp Neurol 61, 197–211. 10.1093/jnen/61.2.197. [PubMed: 11853021]
11. Vaes JEG, Vink MA, de Theije CGM, Hoebeek FE, Benders M, and Nijboer CHA (2019). The Potential of Stem Cell Therapy to Repair White Matter Injury in Preterm Infants: Lessons Learned From Experimental Models. Front Physiol 10, 540. 10.3389/fphys.2019.00540. [PubMed: 31143126]
12. Batalle D, O'Muircheartaigh J, Makropoulos A, Kelly CJ, Dimitrova R, Hughes EJ, Hajnal JV, Zhang H, Alexander DC, Edwards AD, and Counsell SJ (2019). Different patterns of cortical maturation before and after 38 weeks gestational age demonstrated by diffusion MRI in vivo. Neuroimage 185, 764–775. 10.1016/j.neuroimage.2018.05.046. [PubMed: 29802969]
13. Jakovcevski I, and Zecevic N (2005). Sequence of oligodendrocyte development in the human fetal telencephalon. Glia 49, 480–491. 10.1002/glia.20134. [PubMed: 15578660]
14. Back SA, Luo NL, Borenstein NS, Levine JM, Volpe JJ, and Kinney HC (2001). Late oligodendrocyte progenitors coincide with the developmental window of vulnerability for human perinatal white matter injury. J Neurosci 21, 1302–1312. [PubMed: 11160401]
15. Back SA (2017). White matter injury in the preterm infant: pathology and mechanisms. Acta Neuropathol 134, 331–349. 10.1007/s00401-017-1718-6. [PubMed: 28534077]
16. Back SA, Riddle A, and McClure MM (2007). Maturation-dependent vulnerability of perinatal white matter in premature birth. Stroke 38, 724–730. 10.1161/01.STR.0000254729.27386.05. [PubMed: 17261726]

17. Shah DK, Doyle LW, Anderson PJ, Bear M, Daley AJ, Hunt RW, and Inder TE (2008). Adverse neurodevelopment in preterm infants with postnatal sepsis or necrotizing enterocolitis is mediated by white matter abnormalities on magnetic resonance imaging at term. J Pediatr 153, 170–175, 175 e171. 10.1016/j.jpeds.2008.02.033. [PubMed: 18534228]

18. Shah TA, Meinzen-Derr J, Gratton T, Steichen J, Donovan EF, Yolton K, Alexander B, Narendran V, and Schibler KR (2012). Hospital and neurodevelopmental outcomes of extremely low-birth-weight infants with necrotizing enterocolitis and spontaneous intestinal perforation. J Perinatol 32, 552–558. 10.1038/jp.2011.176. [PubMed: 22157625]

19. Paredes MF, James D, Gil-Perotin S, Kim H, Cotter JA, Ng C, Sandoval K, Rowitch DH, Xu D, McQuillen PS, et al. (2016). Extensive migration of young neurons into the infant human frontal lobe. Science 354. 10.1126/science.aaf7073.

20. Sorrells SF, Paredes MF, Cebrian-Silla A, Sandoval K, Qi D, Kelley KW, James D, Mayer S, Chang J, Auguste KI, et al. (2018). Human hippocampal neurogenesis drops sharply in children to undetectable levels in adults. Nature 555, 377–381. 10.1038/nature25975. [PubMed: 29513649]

21. Levison SW, and Goldman JE (1993). Both oligodendrocytes and astrocytes develop from progenitors in the subventricular zone of postnatal rat forebrain. Neuron 10, 201–212. 10.1016/0896-6273(93)90311-e. [PubMed: 8439409]

22. Marshall CA, and Goldman JE (2002). Subpallial dlx2-expressing cells give rise to astrocytes and oligodendrocytes in the cerebral cortex and white matter. J Neurosci 22, 9821–9830. 10.1523/JNEUROSCI.22-22-09821.2002. [PubMed: 12427838]

23. Jiang X, and Nardelli J (2016). Cellular and molecular introduction to brain development. Neurobiol Dis 92, 3–17. 10.1016/j.nbd.2015.07.007. [PubMed: 26184894]

24. Bystron I, Blakemore C, and Rakic P (2008). Development of the human cerebral cortex: Boulder Committee revisited. Nat Rev Neurosci 9, 110–122. 10.1038/nrn2252. [PubMed: 18209730]

25. Lin YY, Welch M, and Lieberman S (2003). The detection of 20(S)-hydroxycholesterol in extracts of rat brains and human placenta by a gas chromatograph/mass spectrometry technique. The Journal of Steroid Biochemistry and Molecular Biology 85, 57–61. 10.1016/s0960-0760(03)00137-7. [PubMed: 12798357]

26. Pataj Z, Liebisch G, Schmitz G, and Matysik S (2016). Quantification of oxysterols in human plasma and red blood cells by liquid chromatography high-resolution tandem mass spectrometry. J Chromatogr A 1439, 82–88. 10.1016/j.chroma.2015.11.015. [PubMed: 26607314]

27. Janowski BA, Willy PJ, Devi TR, Falck JR, and Mangelsdorf DJ (1996). An oxysterol signalling pathway mediated by the nuclear receptor LXR alpha. Nature 383, 728–731. 10.1038/383728a0. [PubMed: 8878485]

28. Lehmann JM, Kliewer SA, Moore LB, Smith-Oliver TA, Oliver BB, Su JL, Sundseth SS, Winegar DA, Blanchard DE, Spencer TA, and Willson TM (1997). Activation of the nuclear receptor LXR by oxysterols defines a new hormone response pathway. J Biol Chem 272, 3137–3140. 10.1074/jbc.272.6.3137. [PubMed: 9013544]

29. Nachtergaele S, Mydock LK, Krishnan K, Rammohan J, Schlesinger PH, Covey DF, and Rohatgi R (2012). Oxysterols are allosteric activators of the oncoprotein Smoothened. Nat Chem Biol 8, 211–220. 10.1038/nchembio.765. [PubMed: 22231273]

30. Nedelcu D, Liu J, Xu Y, Jao C, and Salic A (2013). Oxysterol binding to the extracellular domain of Smoothened in Hedgehog signaling. Nat Chem Biol 9, 557–564. 10.1038/nchembio.1290. [PubMed: 23831757]

31. Rohatgi R, Milenkovic L, and Scott MP (2007). Patched1 regulates hedgehog signaling at the primary cilium. Science 317, 372–376. 10.1126/science.1139740. [PubMed: 17641202]

32. Dwyer JR, Sever N, Carlson M, Nelson SF, Beachy PA, and Parhami F (2007). Oxysterols are novel activators of the hedgehog signaling pathway in pluripotent mesenchymal cells. J Biol Chem 282, 8959–8968. 10.1074/jbc.M611741200. [PubMed: 17200122]

33. Alberta JA, Park SK, Mora J, Yuk D, Pawlitzky I, Iannarelli P, Vartanian T, Stiles CD, and Rowitch DH (2001). Sonic hedgehog is required during an early phase of oligodendrocyte development in mammalian brain. Mol Cell Neurosci 18, 434–441. 10.1006/mcne.2001.1026. [PubMed: 11640898]

34. Ferent J, Zimmer C, Durbec P, Ruat M, and Traiffort E (2013). Sonic Hedgehog signaling is a positive oligodendrocyte regulator during demyelination. J Neurosci 33, 1759–1772. 10.1523/JNEUROSCI.3334-12.2013. [PubMed: 23365216]
35. Gibney SM, and McDermott KW (2009). Sonic hedgehog promotes the generation of myelin proteins by transplanted oligosphere-derived cells. J Neurosci Res 87, 3067–3075. 10.1002/jnr.22138. [PubMed: 19472217]
36. Lu QR, Yuk D, Alberta JA, Zhu Z, Pawlitzky I, Chan J, McMahon AP, Stiles CD, and Rowitch DH (2000). Sonic hedgehog--regulated oligodendrocyte lineage genes encoding bHLH proteins in the mammalian central nervous system. Neuron 25, 317–329. 10.1016/s0896-6273(00)80897-1. [PubMed: 10719888]
37. Ayciriex S, Regazzetti A, Gaudin M, Prost E, Dargere D, Massicot F, Auzeil N, and Laprevote O (2012). Development of a novel method for quantification of sterols and oxysterols by UPLC-ESI-HRMS: application to a neuroinflammation rat model. Anal Bioanal Chem 404, 3049–3059. 10.1007/s00216-012-6396-6. [PubMed: 23010846]
38. Benner EJ, Luciano D, Jo R, Abdi K, Paez-Gonzalez P, Sheng H, Warner DS, Liu C, Eroglu C, and Kuo CT (2013). Protective astrogenesis from the SVZ niche after injury is controlled by Notch modulator Thbs4. Nature 497, 369–373. 10.1038/nature12069. [PubMed: 23615612]
39. Deng Y, Kim B, He X, Kim S, Lu C, Wang H, Cho SG, Hou Y, Li J, Zhao X, and Lu QR (2014). Direct visualization of membrane architecture of myelinating cells in transgenic mice expressing membrane-anchored EGFP. Genesis 52, 341–349. 10.1002/dvg.22751. [PubMed: 24851283]
40. Jin S, Guerrero-Juarez CF, Zhang L, Chang I, Ramos R, Kuan CH, Myung P, Plikus MV, and Nie Q (2021). Inference and analysis of cell-cell communication using CellChat. Nat Commun 12, 1088. 10.1038/s41467-021-21246-9. [PubMed: 33597522]
41. Meng H, Zhang X, Hankenson KD, and Wang MM (2009). Thrombospondin 2 potentiates notch3/jagged1 signaling. J Biol Chem 284, 7866–7874. 10.1074/jbc.M803650200. [PubMed: 19147503]
42. Laferriere F, Maniecka Z, Perez-Berlanga M, Hruska-Plochan M, Gilhespy L, Hock EM, Wagner U, Afroz T, Boersema PJ, Barmettler G, et al. (2019). TDP-43 extracted from frontotemporal lobar degeneration subject brains displays distinct aggregate assemblies and neurotoxic effects reflecting disease progression rates. Nat Neurosci 22, 65–77. 10.1038/s41593-018-0294-y. [PubMed: 30559480]
43. Nagao M, Lanjakornsiripan D, Itoh Y, Kishi Y, Ogata T, and Gotoh Y (2014). High mobility group nucleosome-binding family proteins promote astrocyte differentiation of neural precursor cells. Stem Cells 32, 2983–2997. 10.1002/stem.1787. [PubMed: 25069414]
44. Kase ET, Andersen B, Nebb HI, Rustan AC, and Thoresen GH (2006). 22-Hydroxycholesterols regulate lipid metabolism differently than T0901317 in human myotubes. Biochim Biophys Acta 1761, 1515–1522. 10.1016/j.bbalip.2006.09.010. [PubMed: 17055780]
45. Svensson S, Ostberg T, Jacobsson M, Norstrom C, Stefansson K, Hallen D, Johansson IC, Zachrisson K, Ogg D, and Jendeberg L (2003). Crystal structure of the heterodimeric complex of LXRalpha and RXRbeta ligand-binding domains in a fully agonistic conformation. EMBO J 22, 4625–4633. 10.1093/emboj/cdg456. [PubMed: 12970175]
46. Zuercher WJ, Buckholz RG, Campobasso N, Collins JL, Galardi CM, Gampe RT, Hyatt SM, Merrihew SL, Moore JT, Oplinger JA, et al. (2010). Discovery of tertiary sulfonamides as potent liver X receptor antagonists. J Med Chem 53, 3412–3416. 10.1021/jm901797p. [PubMed: 20345102]
47. Nery S, Wichterle H, and Fishell G (2001). Sonic hedgehog contributes to oligodendrocyte specification in the mammalian forebrain. Development 128, 527–540. 10.1242/dev.128.4.527. [PubMed: 11171336]
48. Ortega JA, Radonjic NV, and Zecevic N (2013). Sonic hedgehog promotes generation and maintenance of human forebrain Olig2 progenitors. Front Cell Neurosci 7, 254. 10.3389/fncel.2013.00254. [PubMed: 24379757]
49. Lauth M, Bergstrom A, Shimokawa T, and Toftgard R (2007). Inhibition of GLI-mediated transcription and tumor cell growth by small-molecule antagonists. Proc Natl Acad Sci U S A 104, 8455–8460. 10.1073/pnas.0609699104. [PubMed: 17494766]

50. Bai CB, and Joyner AL (2001). Gli1 can rescue the in vivo function of Gli2. Development 128, 5161–5172. 10.1242/dev.128.24.5161. [PubMed: 11748151]
51. Wynn JL, Scumpia PO, Delano MJ, O'Malley KA, Ungaro R, Abouhamze A, and Moldawer LL (2007). Increased mortality and altered immunity in neonatal sepsis produced by generalized peritonitis. Shock 28, 675–683. 10.1097/SHK.0b013e3180556d09. [PubMed: 17621256]
52. Wynn JL, Scumpia PO, Winfield RD, Delano MJ, Kelly-Scumpia K, Barker T, Ungaro R, Levy O, and Moldawer LL (2008). Defective innate immunity predisposes murine neonates to poor sepsis outcome but is reversed by TLR agonists. Blood 112, 1750–1758. 10.1182/blood-2008-01-130500. [PubMed: 18591384]
53. Liu C, Li W, Johnson GA, and Wu B (2011). High-field (9.4 T) MRI of brain dysmyelination by quantitative mapping of magnetic susceptibility. Neuroimage 56, 930–938. 10.1016/j.neuroimage.2011.02.024. [PubMed: 21320606]
54. Lee J, Shmueli K, Kang BT, Yao B, Fukunaga M, van Gelderen P, Palumbo S, Bosetti F, Silva AC, and Duyn JH (2012). The contribution of myelin to magnetic susceptibility-weighted contrasts in high-field MRI of the brain. Neuroimage 59, 3967–3975. 10.1016/j.neuroimage.2011.10.076. [PubMed: 22056461]
55. Zhong K, Ernst T, Buchthal S, Speck O, Anderson L, and Chang L (2011). Phase contrast imaging in neonates. Neuroimage 55, 1068–1072. 10.1016/j.neuroimage.2010.11.086. [PubMed: 21232619]
56. Lagace DC, Whitman MC, Noonan MA, Ables JL, DeCarolis NA, Arguello AA, Donovan MH, Fischer SJ, Farnbauch LA, Beech RD, et al. (2007). Dynamic contribution of nestin-expressing stem cells to adult neurogenesis. J Neurosci 27, 12623–12629. 10.1523/JNEUROSCI.3812-07.2007. [PubMed: 18003841]
57. Billiards SS, Haynes RL, Folkerth RD, Borenstein NS, Trachtenberg FL, Rowitch DH, Ligon KL, Volpe JJ, and Kinney HC (2008). Myelin abnormalities without oligodendrocyte loss in periventricular leukomalacia. Brain Pathol 18, 153–163. 10.1111/j.1750-3639.2007.00107.x. [PubMed: 18177464]
58. Buser JR, Maire J, Riddle A, Gong X, Nguyen T, Nelson K, Luo NL, Ren J, Struve J, Sherman LS, et al. (2012). Arrested preoligodendrocyte maturation contributes to myelination failure in premature infants. Ann Neurol 71, 93–109. 10.1002/ana.22627. [PubMed: 22275256]
59. Back SA, Luo NL, Mallinson RA, O'Malley JP, Wallen LD, Frei B, Morrow JD, Petito CK, Roberts CT Jr., Murdoch GH, and Montine TJ (2005). Selective vulnerability of preterm white matter to oxidative damage defined by F2-isoprostanes. Ann Neurol 58, 108–120. 10.1002/ana.20530. [PubMed: 15984031]
60. Truttmann AC, Ginet V, and Puyal J (2020). Current Evidence on Cell Death in Preterm Brain Injury in Human and Preclinical Models. Front Cell Dev Biol 8, 27. 10.3389/fcell.2020.00027. [PubMed: 32133356]
61. Samanta J, Grund EM, Silva HM, Lafaille JJ, Fishell G, and Salzer JL (2015). Inhibition of Gli1 mobilizes endogenous neural stem cells for remyelination. Nature 526, 448–452. 10.1038/nature14957. [PubMed: 26416758]
62. Tong CK, Fuentealba LC, Shah JK, Lindquist RA, Ihrie RA, Guinto CD, Rodas-Rodriguez JL, and Alvarez-Buylla A (2015). A Dorsal SHH-Dependent Domain in the V-SVZ Produces Large Numbers of Oligodendroglial Lineage Cells in the Postnatal Brain. Stem Cell Reports 5, 461–470. 10.1016/j.stemcr.2015.08.013. [PubMed: 26411905]
63. Brown JVE, Walsh V, and McGuire W (2019). Formula versus maternal breast milk for feeding preterm or low birth weight infants. Cochrane Database Syst Rev 8, CD002972. 10.1002/14651858.CD002972.pub3. [PubMed: 31452191]
64. Blesa M, Sullivan G, Anblagan D, Telford EJ, Quigley AJ, Sparrow SA, Serag A, Semple SI, Bastin ME, and Boardman JP (2019). Early breast milk exposure modifies brain connectivity in preterm infants. Neuroimage 184, 431–439. 10.1016/j.neuroimage.2018.09.045. [PubMed: 30240903]
65. Deoni SC, Dean DC 3rd, Piryatinsky I, O'Muircheartaigh J, Waskiewicz N, Lehman K, Han M, and Dirks H (2013). Breastfeeding and early white matter development: A cross-sectional study. Neuroimage 82, 77–86. 10.1016/j.neuroimage.2013.05.090. [PubMed: 23721722]

66. Lechner BE, and Vohr BR (2017). Neurodevelopmental Outcomes of Preterm Infants Fed Human Milk: A Systematic Review. Clin Perinatol 44, 69–83. 10.1016/j.clp.2016.11.004. [PubMed: 28159210]

67. Section on, B. (2012). Breastfeeding and the use of human milk. Pediatrics 129, e827–841. 10.1542/peds.2011-3552. [PubMed: 22371471]

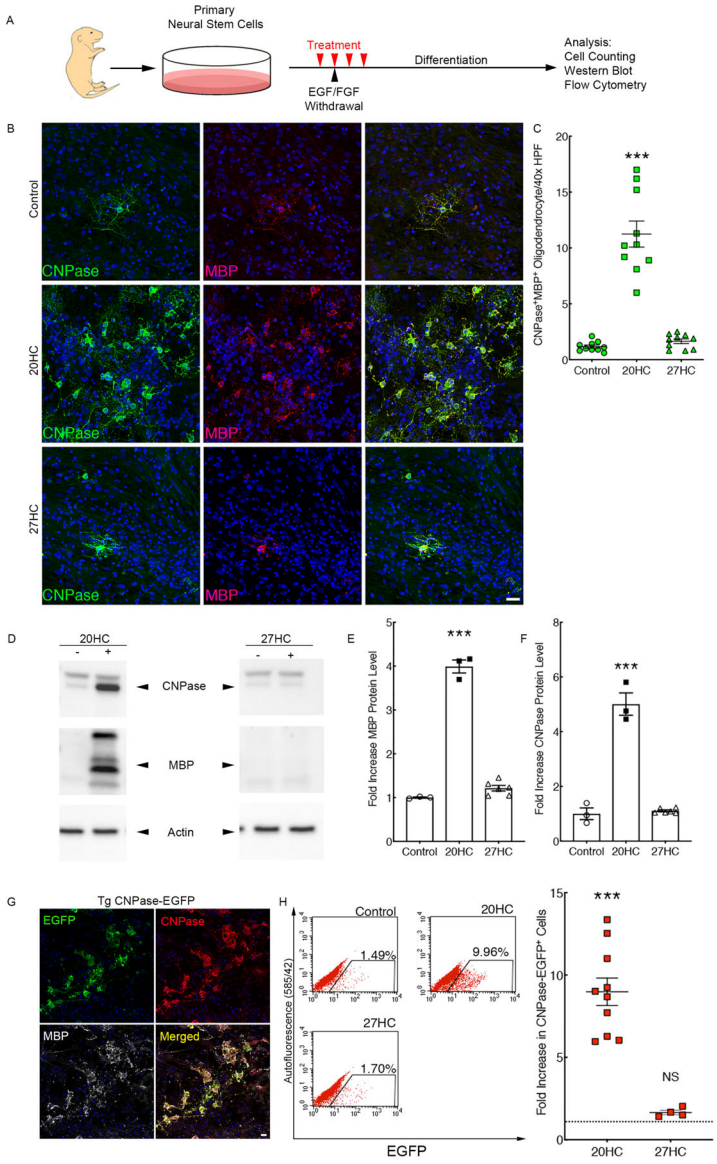

Figure 1. 20HC induces oligodendrocyte differentiation in NSPCs *in vitro*.

A, Experimental design. SVZ-derived NSPCs were propagated in EGF and FGF. 24 hours before growth factor withdrawal cells were treated with media or indicated oxysterol for 3 days. Analysis was performed 15 days after growth factor withdrawal.

B, Images of differentiated NSPCs treated with vehicle control, 1μM 20HC, or 1μM 27HC. Cells were stained for CNPase (green) and myelin basic protein (MBP, red). Scale bar=25μm.

C, Numbers of $CNPase^{+}MBP^{+}$ oligodendrocytes/high powered field (HPF). Each data point represents an independent experiment. Mean±SEM. One-way ANOVA followed by Bonferroni's multiple comparisons test. ***P<0.0001.

D, Protein lysates from differentiated NSPC cultures treated with 1μM of 20HC or 27HC were probed for CNPase, MBP, and actin.

E,F MBP or CNPase levels normalized to actin and presented as fold increase over vehicle (DMSO) controls. Mean±SEM. One-way ANOVA followed by Bonferroni's multiple comparisons test. ***P<0.0001.

G, Images of transgenic CNPase-EGFP 20HC-treated NSPCs immunostained for EGFP (green), CNPase (red) or MBP (white). Scale bar = 10μm.

H, Representative flow cytometric analysis of 15-day differentiated NSPCs from transgenic CNPase-EGFP mice analyzed for EGFP expression following treatment with indicated oxysterol at 1μM. Percent $EGFP^+$ cells are indicated in individual plots. Average flow cytometric analysis represented as fold-increase over controls (dashed line). Each point is an independent experiment. One-way ANOVA followed by Bonferroni's multiple comparisons test. ***P<0.0001. Non-significance is indicated by NS.

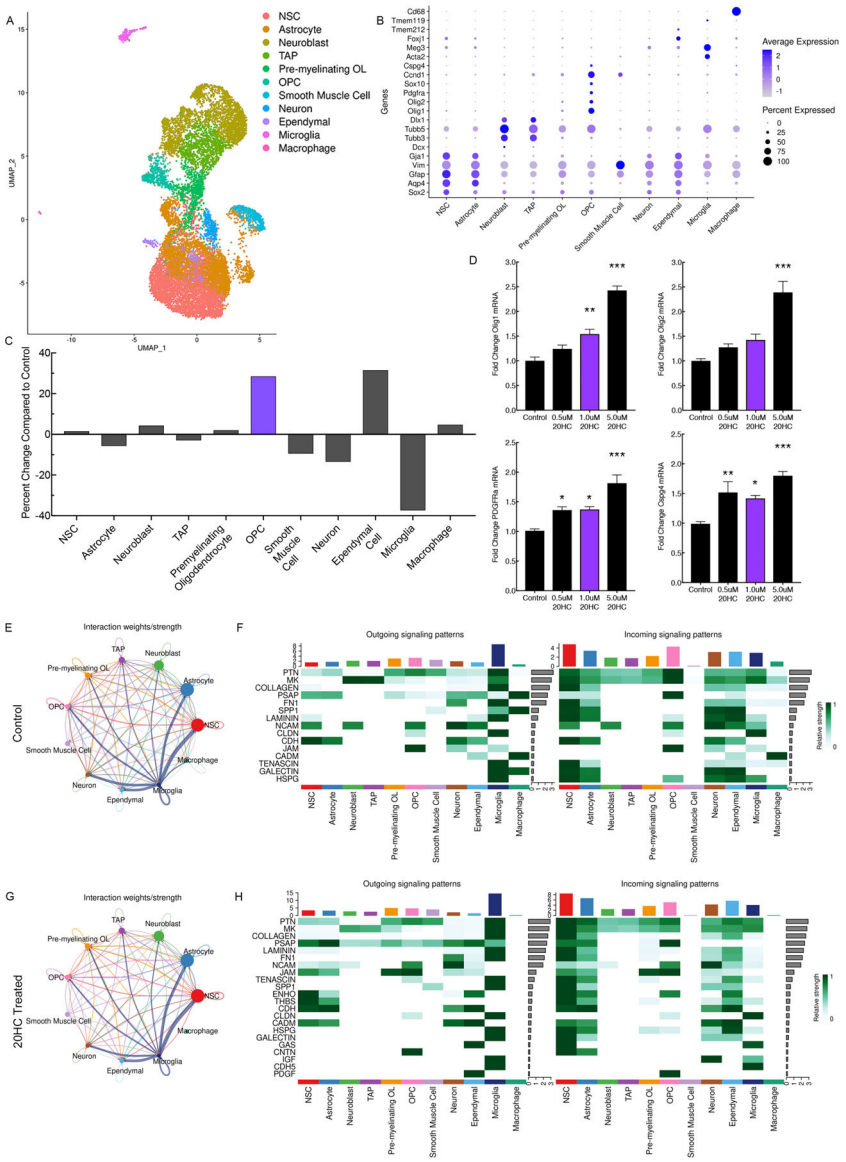

Figure 2. Single cell sequencing of NSPCs treated with 20HC.

A, UMAP plot showing gene expression relationships among 10,730 cells in the control group with 6,052 individual genes profiled. 11 different clusters are color coded.

B, Dot plot representation of original sample source with genes corresponding to each cluster.

C, Change in cell cluster size after 20HC-treatment at day 3 of differentiation. Percent change represents the change in size of indicated cluster relative to the entire cell population for 20HC treatment compared to control. OPC cluster shown in purple.

D, Escalating 20HC dose effect on fold change in *Olig1, Olig2, PDGFRa* and *Cspg4* transcripts by qPCR compared to vehicle control on day 3 of treatment. Purple bar indicates 1μM dosing matching the dose used in single cell analysis. Results are the average of 12 NSPC samples/condition representing 3 independent experiments. Oneway ANOVA followed by Bonferroni's multiple comparisons test. Mean±SEM. *P<0.05,

**P<0.001, ***P<0.0001.

E, CellChat displaying unbiased interactions between clusters in the control group, with increased line thickness correlating with strength of interaction.

F, Specific outgoing and incoming (ligand-receptor) signaling patterns within each cluster as represented in (E).

G, CellChat displaying unbiased interactions between clusters in the 20HC-treated group, with increased line thickness correlating with strength of interaction.

H, Specific outgoing and incoming (ligand-receptor) signaling patterns within each cluster as represented in (G).

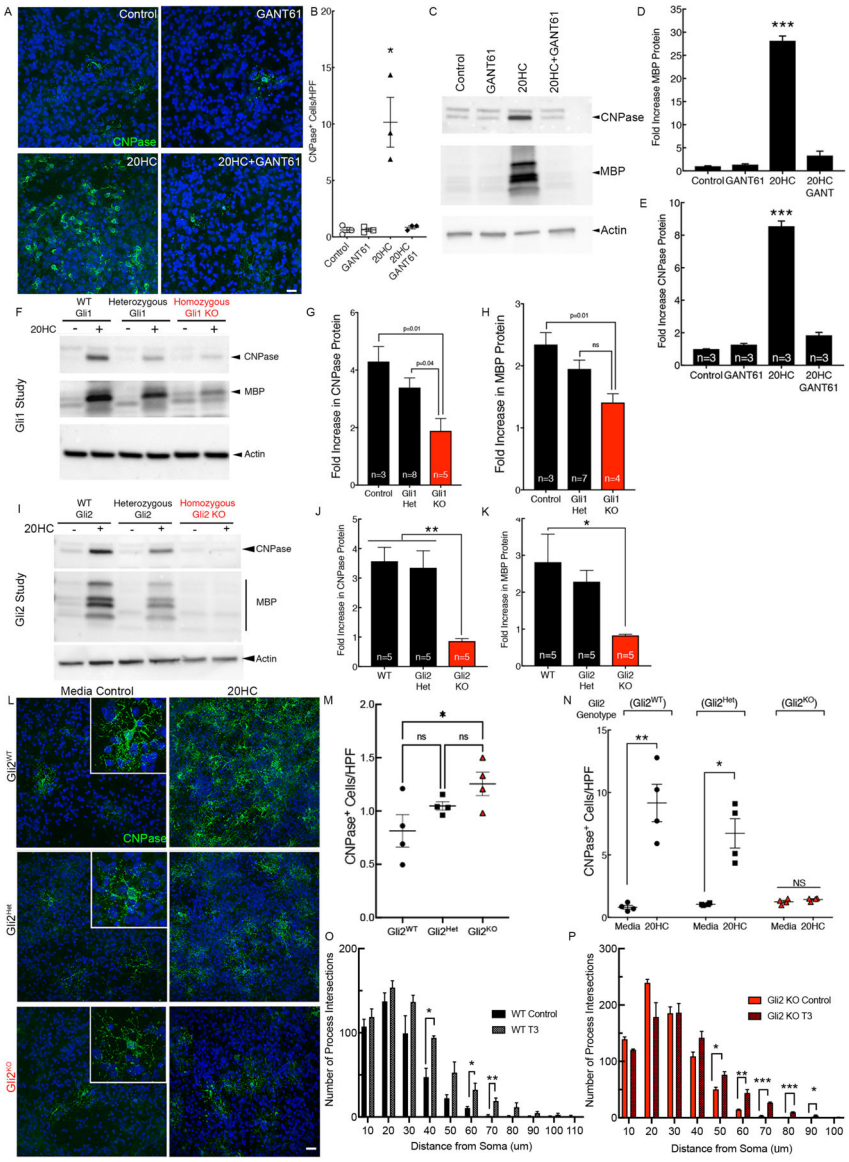

Figure 3. Oxysterol-induced oligodendrogenesis is Gli-dependent.

A, Images of differentiated NSPCs treated with vehicle control, 5μM GANT61, 1μM 20HC, or 20HC+GANT61. CNPase (green) and DAPI (blue). Scale bar = 10μm.

B, Numbers of CNPase$^+$ oligodendrocytes/high powered field (HPF). Each point represents an independent experiment. Mean±SEM. One-way ANOVA followed by Bonferroni's multiple comparisons test. *P < 0.05.

C, 15-day differentiated NSPC lysates from vehicle control, 5μM GANT61, 1μM 20HC, or 20HC+GANT61 were probed for CNPase, MBP, or actin.

D, E, MBP or CNPase levels normalized to actin and presented as fold increase over vehicle controls. Mean±SEM for 3 experiments. One-way ANOVA followed by Bonferroni's multiple comparisons test. ***P<0.0001.

F, NSPCs from Gli1 wild type (WT), Gli1 heterozygotes (Gli1 Het) and Gli1 knockout (Gli1 KO) were treated with vehicle or 1μM 20HC and differentiated for 15 days. Protein lysates were probed for CNPase, MBP, or actin. Representative immunoblot shown.

G,H MBP or CNPase levels normalized to actin and presented as fold increase over vehicle controls for Gli1 genotypes. Mean±SEM. One-way ANOVA followed by Bonferroni's multiple comparisons test. *P < 0.05; **P < 0.01.

I, NSPCs from Gli2 wild type (WT), Gli2 heterozygotes (Gli2 Het) and Gli2 knockout (Gli2 KO) were treated with vehicle or 1μM 20HC and differentiated for 15 days. Protein lysates were probed for CNPase, MBP, or actin. Representative immunoblot shown.

J,K MBP or CNPase levels normalized to actin and presented as fold increase over vehicle controls for Gli2 genotypes. Mean±SEM. One-way ANOVA followed by Bonferroni's multiple comparisons test. *P < 0.05; **P < 0.01.

L, NSPCs from Gli2 genotypes from control or 1μM 20HC were immunostained on day 15 for CNPase (green) and dapi (blue). Scale bar = 25μm.

M, Number of $CNPase^+$ cells in Gli2WT, Gli2Het, and Gli2KO following differentiation of NSPCs in control media. Represented as $CNPase^+$ cells/high powered field (HPF). Mean±SEM. One-way ANOVA followed by Bonferroni's multiple comparisons test. *P<0.05.</p/>N, Number of $CNPase^+$ cells in each Gli2 genotype in media control compared to 1μM 20HC treated cultures. Results are the average from 3–4 mice per genotype. Unpaired Student's t test. *P < 0.05; **P < 0.01.

O, Sholl analysis of oligodendrocyte morphology from $Gli2^{WT}$ NSPCs following treatment with vehicle or T3. Cell staining for CNPase and Sholl analysis performed at day 12. Unpaired Student's t test. *P < 0.05; **P < 0.01.

P, Sholl analysis of oligodendrocyte morphology from $Gli2^{WT}$ NSPCs following treatment with vehicle or T3. Cell staining for CNPase and Sholl analysis performed at day 12. . Unpaired Student's t test. *P < 0.05; **P < 0.01, ***P<0.0001.

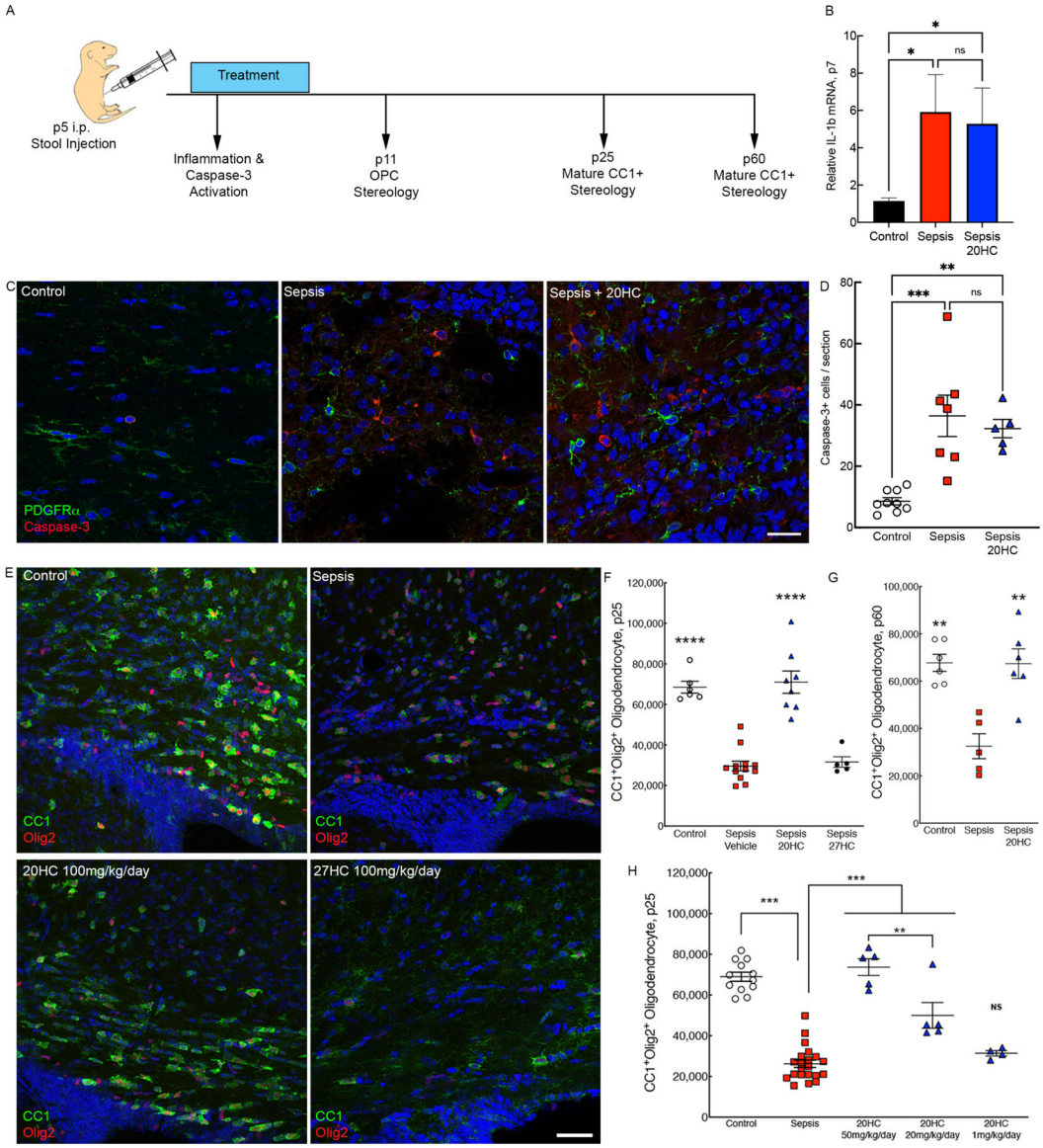

Figure 4. 20HC treatment rescues oligodendrocyte numbers following neonatal WMI.

A, Schematic overview of experimental treatment and analysis.

B, qPCR analysis of IL-1β from control, sepsis, and sepsis+20HC mice in brain tissue 2 days after sepsis. Mean±SEM. One-way ANOVA followed by Bonferroni's multiple comparisons test. *P<0.05. Non-significance is indicated by NS.

C, Mice were injected with cecal slurry on p5 and treated with vehicle or 20HC. On p7, control, sepsis+vehicle, sepsis+20HC (100mg/kg/day) were immunostained for activated caspase-3^+ and PDGFRα+ cells in the periventricular white matter regions.

D, Caspase-3^+ cells were counted in the CC and the cortex. Data presented as caspase-3^+ cells/section. Each dot represents counts for an individual mouse. Mean±SEM. One-way ANOVA followed by Bonferroni's multiple comparisons test. ** P<0.01, *** P<0.001. Non-significance is indicated by NS.

E, Representative images of CC1 and Olig2 immunostained tissue in the CC from control, sepsis + vehicle, and septic + 20HC or 27HC. Scale bar = 50μm.

F, Total numbers of $CC1^{+}Olig2^{+}$ oligodendrocytes on p25. Mean±SEM. One-way ANOVA followed by Bonferroni's multiple comparisons test. ****$P<0.0001$

G, Total numbers of $CC1^{+}Olig2^{+}$ oligodendrocytes on p60. Mean±SEM. One-way ANOVA followed by Bonferroni's multiple comparisons test. **$P<0.01$

H, Dose response to 20HC (50, 20, and 1 mg/kg/day). Total numbers of $CC1^{+}Olig2^{+}$ oligodendrocytes on p25. Mean±SEM. One-way ANOVA followed by Bonferroni's multiple comparisons test. **$P<0.01$, ***$P<0.001$. Non-significance is indicated by NS.

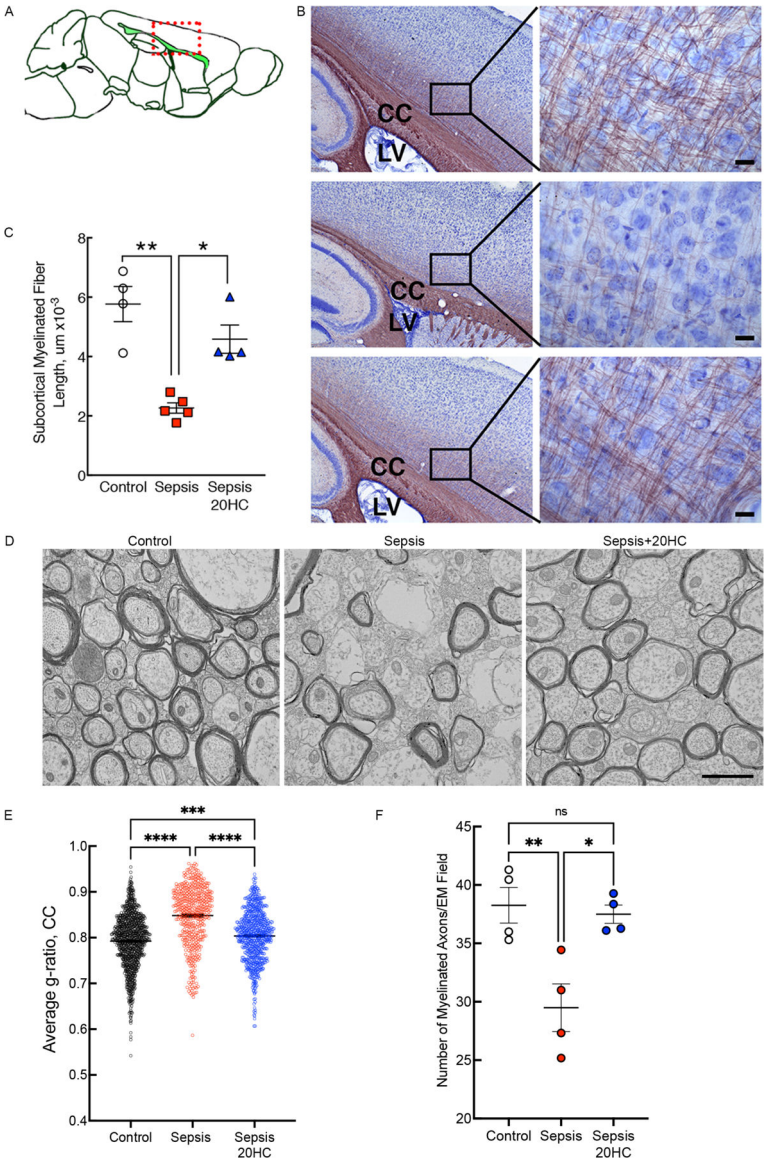

Figure 5. 20HC improves myelination following neonatal WMI.

A, Sagittal section schematic for orientation to region of interest (red dashed box) shown in (B).

B, Representative Black Gold and Nissl staining imaged at 5x (left). Ventricle (LV) and corpus callosum (CC) are shown. Boxed area of subcortical white matter was imaged at 63x (right). Bar = 10μm.

C, Stereological space ball probe estimating end to end length of myelinated fibers for control (n=4 mice), sepsis (n=5 mice), and sepsis+20HC (n=4 mice). 4 sections/mouse were analyzed. Mean ±SEM. One-way ANOVA followed by Bonferroni testing. *P<0.05, **P<0.01.

D, Electron microscopy in sagittal sections of the midline CC. Representative EM images in control, sepsis and sepsis+20HC-treated mice. Black bar = 500nm

E, g-ratios grouped by treatment group. Mean ±SEM. One-way ANOVA followed by Bonferroni testing. ***P<0.001, ****P<0.0001.

F, Total number of myelinated axons per 50 μm^2 were counted for control (n=4 mice), sepsis (n=3 mice), and sepsis+20HC (n=4 mice). Mean ±SEM. One-way ANOVA followed by Bonferroni testing. *P<0.05, **P<0.01. Non-significance is indicated by NS.

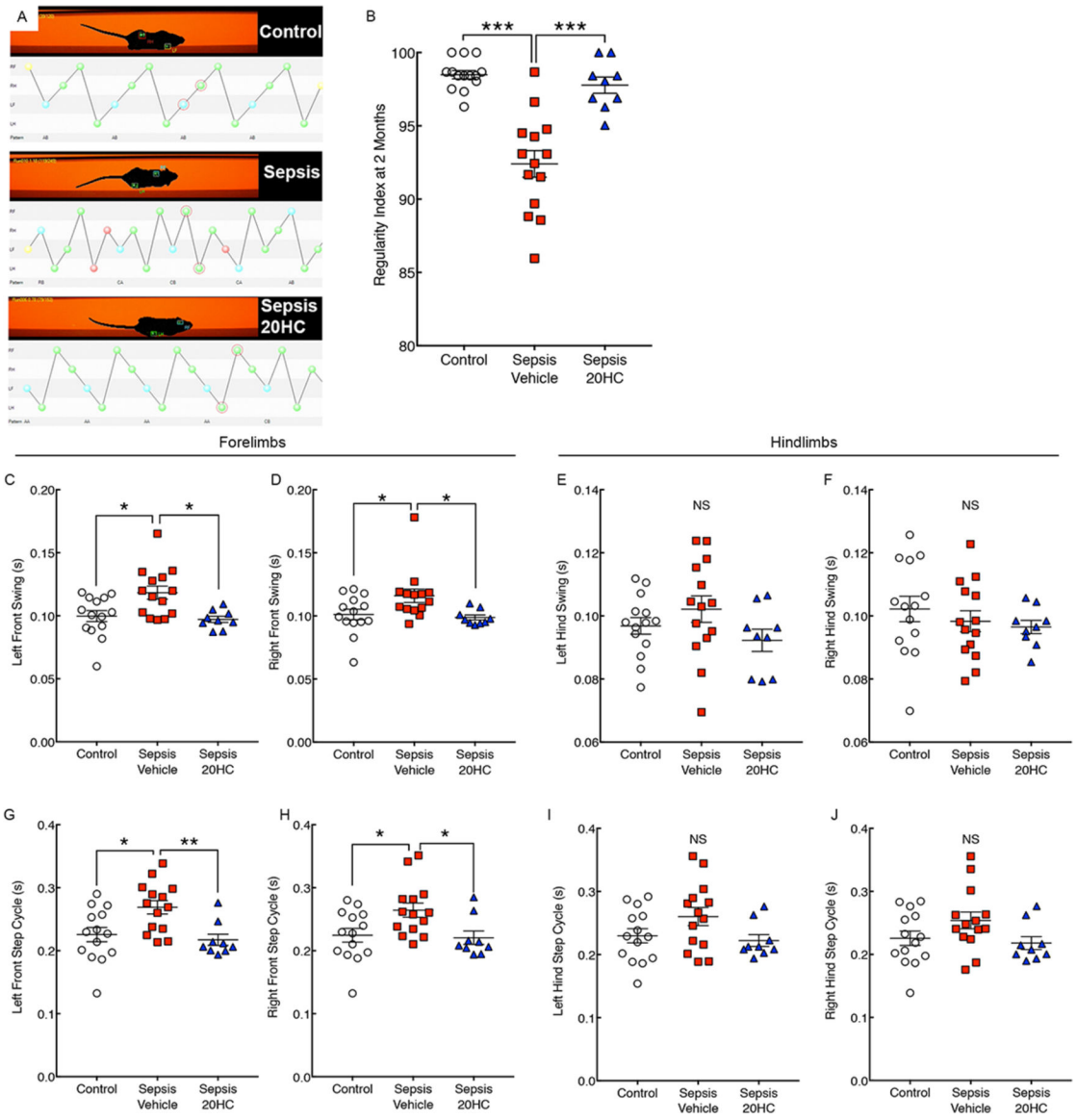

Figure 6. 20HC improves motor outcomes following neonatal WMI.

A, Gait analysis on 2-month-old mice following neonatal injury ± treatment. (see Video S1). Red dots indicate a misplaced paw step.

B, Regularity index. Dots represent individual mice. Mean±SEM. One-way ANOVA followed by Bonferroni's multiple comparisons test.

C, Average results for left front swing time.</p/>D, Average results for right front swing time.</p/> E, Average results for left hind swing time.

F, Average results for right hind swing time.

G, Average results for left front step cycle time.</p/>H, Average results for right front step cycle time.</p/> I, Average results for left hind step cycle time.

J, Average results for right hind step cycle time.

Control mice (open circles, n=14), sepsis (red squares, n=14) or sepsis+20HC treatment (blue triangles, n=9). One-way ANOVA followed by Bonferroni's multiple comparisons

test (B) or Tukey's multiple comparisons test (C to J). *P<0.01, **P<0.001, ***P<0.0001. Non-significance is indicated by NS.

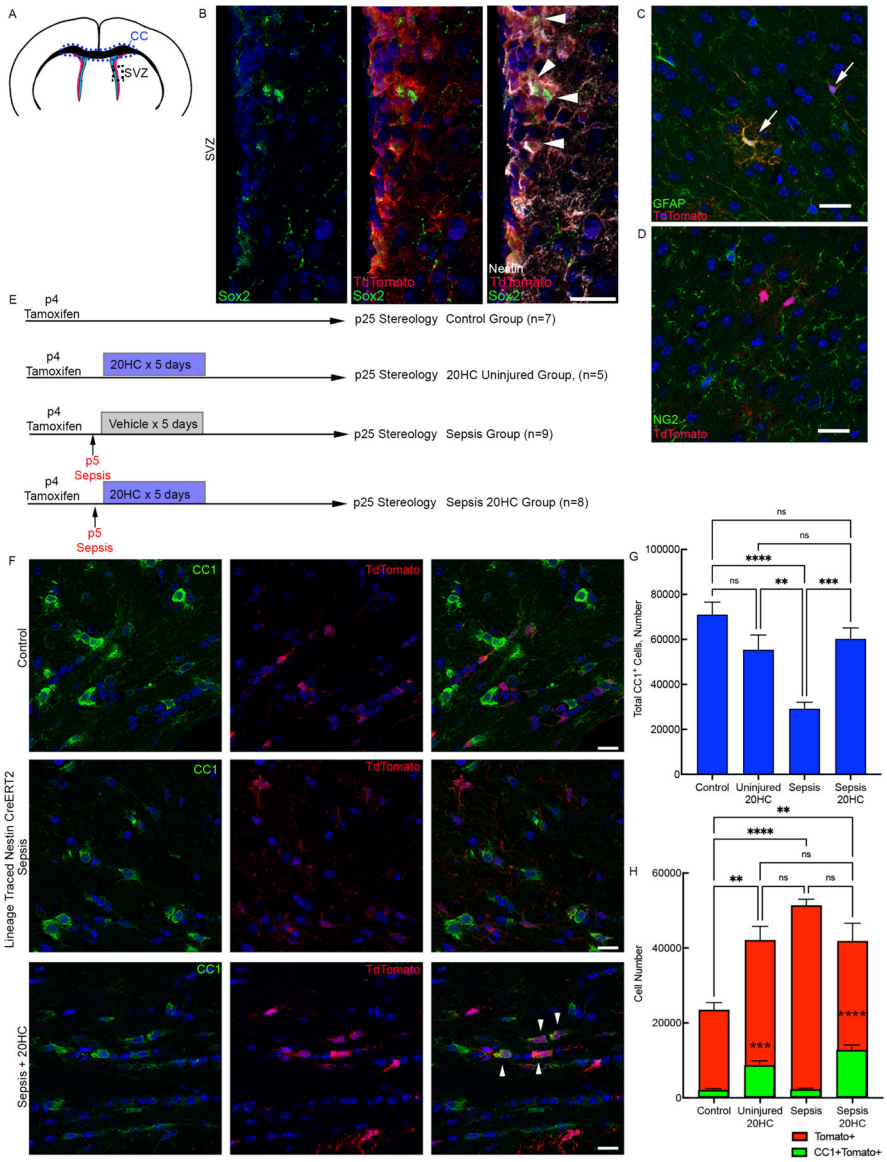

Figure 7. 20HC induces SVZ-derived oligodendrogenesis *in vivo* after neonatal WMI.

A, Schematic representation of the subventricular zone (SVZ), corpus callosum (CC), and lateral ventricle (LV) in coronal section.

B, Nestin-CreER^{T2};R26r-TdTomato mice were injected with tamoxifen on p4. After 3 days, the coronal sections through the SVZ was immunostained with anti-Sox-2 (green), anti-RFP (TdTomato, red), and anti-nestin (white). Scale bar = 25μm.

C, TdTomato (red) colocalized with GFAP^{+} astrocytes (green, arrows) in the periventricular white matter.

D, NG2^{+} OPCs (green) do not colocalize with TdTomato (red).

E, Overview of SVZ NSPC lineage tracing experiment.

F, Representative images of p25 tissue immunostained for oligodendrocyte marker CC1 (green) and TdTomato from control, sepsis, and sepsis + 20HC groups. Arrowheads indicate colocalization. Bar = 25μm.

G, Total number of $CC1^+$ oligodendrocytes obtained by stereology. Mean ± SEM. Mean ± SEM. One-way ANOVA followed by Bonferroni's multiple comparisons test. **P<0.01, ***P<0.001, ****P<0.0001.

H, Number of $TdTomato^+$ cells (red) and $CC1^+TdTomato^+$ cells (green). $CC1^+TdTomato^+$ cells are lineage traced SVZ-derived oligodendrocytes. Mean ± SEM. One-way ANOVA followed by Bonferroni's multiple comparisons test. **P<0.01, ****P<0.0001.